CrossMark

Quantification of the Dynamic Compressive Response of Two Ottawa Sands

Y. Lin[1,2] · W. Yao[2] · M. Jafari[2] · N. Wang[3] · K. Xia[2]

Abstract Two types of Ottawa sand (ASTM C778 #20–30 graded sand, denoted OS1, and C109 ASTM #C778 graded sand, denoted OS2) with different particle size distributions were tested in a series of dynamic uniaxial strain experiments using a modified split Hopkinson pressure bar (SHPB) system. The pulse shaper technique was employed to achieve the dynamic force balance and constant strain rate in the sand specimen. The effects of the strain rate, initial void ratio and moisture on the dynamic compression response of sand were examined. Two types of dynamic behavior occurred in the dry sand: solid-like and fluid-like behavior. The OS1 samples exhibited a fluid-like response at all initial void ratios, whereas the OS2 samples exhibited a solid-like response for all void ratios. This difference between the two sands may be due to the difference in the particular size distributions of OS1 and OS2. The initial elastic response of the dry sand samples seemed to be independent of the strain rate. The strain rate effects became more apparent after particle crushing and particle rearrangement began. Under a high degree of saturation, the strain rate effects were immediately apparent, even at lower strains. The dynamic response of sand was remarkably linear until the peak strain was reached.

Introduction

The effect of strain rate plays a significant role in the load-deformation response of materials in many geotechnical applications. Stiffness and strength are often dependent on the strain rate sustained during the loading period. This rate dependence extends from slowly applied strains (10^{-6} s^{-1}) during the construction of a large structure to rapidly applied strains (10^6 s^{-1}) during blasting [1]. At high strain rates, materials tend to exhibit higher strength, greater stiffness, and lower strain before failure. To accurately model the response of soil in blasting, impact, dynamic compaction, and other applications, rigorous and well-defined testing methodologies must be developed to properly quantify the soil's material parameters.

The stress-strain response of sand under confinement is complex, and an increased degree of saturation plays a key role in this response. The effect of confinement on the stress-strain response of dry sand under uniaxial strain is schematically illustrated in Fig. 1. As the confinement increases, the soil response becomes stiffer due to the enhanced friction between sand particles. After an initial elastic response and yielding of the soil skeleton, a hardening and lock-up phase dominates, which is characterized by an increase in stiffness relative to the yielding phase. Finally, energy-intensive particle crushing begins and leads to further increases in the stiffness as the void spaces become occupied by progressively finer sand particles. Under an extremely high confining pressure, the crushed particles are in a state featuring more contacts, resulting in a pseudo-elastic behavior approaching that of sandstone. In contrast to dry sand samples, the majority of

✉ K. Xia
kaiwen.xia@utoronto.ca

1 Scientific College, National University of Defense Technology, Changsha, Hunan 410073, China

2 Department of Civil Engineering, University of Toronto, Toronto, ON M5S 1A4, Canada

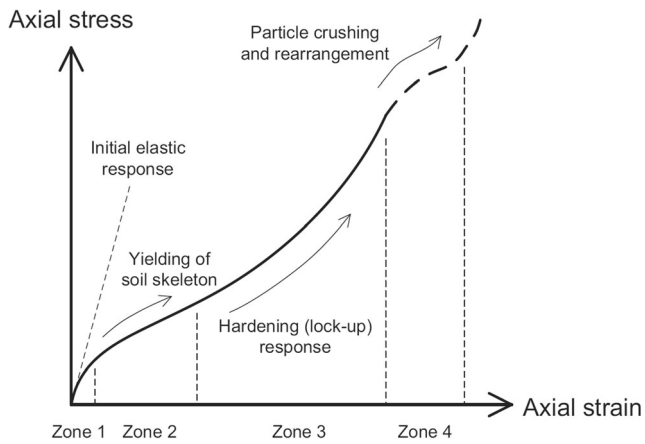3 Department of Civil Engineering, Beihang University, Beijing 100191, China

Fig. 1 Stress-strain curve of dry sand under uniaxial strain loading (Omidvar et al. [2] redrawn from Whitman [5])

the voids in high-saturation sand samples are filled with water and sand and thus exhibit lower compressibility. Because water cannot be drained during the loading process under a high strain rate, the deformation of sand is determined by the deformation of water (and a small amount of air), and the deformation of the solid phase becomes significant when a high confining pressure is reached.

Omidvar et al. [2] presented a comprehensive summary of the different uniaxial compression tests performed under high strain rates. Several approaches have been taken to apply a high-strain-rate load to a soil or sand sample, such as the drop weight systems [3], gas-driven pistons [4], hydraulic-driven pistons [5] and explosive-loaded pistons [6]. As one of the powerful tools used to study material responses, the split Hopkinson pressure bar (SHPB) has been modified in recent decades to study the behavior of granular materials under different loading conditions [7–13]. Pierce and Charlie [14] placed samples in a deformable membrane within a larger cylinder. Pressurized water was pumped into the cylinder to control the radial confining pressure in the sample. Martin et al. [15] and Kabir and Chen [16] reported triaxial SHPB tests on sand with confining pressures of up to 150 MPa. In these tests, a pressurized cylinder was applied over the sample and at the end of the transmitted bar to maintain a hydrostatic pressure in the sample. The deviatoric stress was then applied dynamically via the impact of the striker bar. Song et al. [17] described another approach to confine the sand sample, in which a stiff steel jacket was placed outside the sample to provide confinement in the radial direction. Because of the large difference in stiffness between the jacket and sand sample, the confinement can be considered rigid, and the deformation of the sand is essentially one-dimensional strain.

Although many studies have performed dynamic testing, many questions regarding the behavior of sand remain unresolved. The material behavior of sand under high strain rates is still not fully understood for varying degrees of saturation, initial void ratios, particle shape and size distributions, surface textures, and mineralogies. In this paper, two types of Ottawa

sand under a high degree of saturation and a dry condition are tested at high strain rates using a modified SHPB method following Song et al. [17]. The pulse shaper technique is used to achieve the dynamic force balance and constant strain rate. The effects of the particle size distribution, initial void ratio, and degree of saturation on the dynamic responses of sand are obtained, and two types of responses of sand are observed, namely, fluid-like and solid-like responses.

Experimental Procedure

Materials

The two types of Ottawa sand considered in this study are both pure quartz sand commercially available from Ottawa, Illinois. A fine-grained Ottawa sand (OS1) is a silica classified ASTM C778 #20–30 sand, and a coarse-grained Ottawa sand (OS2) is a silica classified C109 ASTM #C778 graded sand. OS1 and OS2 are tested to examine the effect of particle size distribution on the material response of sand. The particle densities of OS1 and OS2 are 2.635 and 2.653 g/cm^3, respectively. The sieve analysis results for both sands are provided in Table 1, and the particle size distribution is shown in Fig. 2. The D50 values for OS1 and OS2 are 0.4 mm and 0.88 mm, respectively.

Experimental Setup

The sand samples were subjected to a variety of dynamic tests in a modified SHPB loading system, and a quasi-static test using a similar sample configuration was conducted in a hydraulic servo-controlled testing system.

A 25.4-mm-diameter SHPB system was used in the dynamic tests. The system comprises a 200-mm-long single striker bar, a 2000-mm-long incident bar, and a 1200-mm-long transmitted bar. All bars are made of high-strength maraging steel with a Young's modulus of 200 GPa and a yield strength of 2.5 GPa. Pairs of diametrically oriented strain gauges were placed on the surface of the incident and transmitted bars, each at 1000 mm and 500 mm away from the sample interface, respectively. An eight-channel Sigma digital oscilloscope manufactured by Nicolet Instrument Technologies, Madison, WI, USA was used to record and store the amplified strain signals collected from the Wheatstone bridge circuits.

During the test, the sand sample is placed between the incident and transmitted bars, and the striker is launched to impact the incident bar (Fig. 3). An incident stress wave is generated and propagates through the incident bar and into the sample. At the location of the sample, the incident wave is divided into a reflected wave propagating back into the incident bar and a transmitted wave into the transmitted bar. A maraging steel sleeve with internal and external diameters of 25.4 mm and 35.4 mm, respectively, is used to provide passive

Table 1 Particle size distribution of the two types of Ottawa sand

Size (mm)	OS1			OS2		
	Mass (g)	Percent (%)	Percent passing (%)	Mass (g)	Percent (%)	Percent passing (%)
1.18	0	0	100	0.1	0.0236	99.97
0.60	1.12	0.1840	99.816	417.9	98.8083	1.1681
0.30	470.31	77.2545	22.5615	4.92	1.1633	0.0048
0.18	129.13	21.2113	1.3502	0.02	0.0048	0
0.15	6.09	1.0004	0.3498	0	0	0
0.106	1.62	0.2660	0.0838	0	0	0
0.075	0.31	0.0509	0.0329	0	0	0
0.053	0.13	0.0214	0.0115	0	0	0
Total	608.78	100		422.94	100	

confinement to the sand sample. Because the relative stiffness of the steel is considerably larger than that of the sand material, it can be assumed that the sample is in a state of uniaxial strain during the test. The sample assembly is attached to the bar system using two sliding fit plastic rings.

Using the strain history data of the three waves recorded by each pair of strain gauges, the load-deformation response of the sand sample can be calculated under the assumptions of one-dimensional stress propagation through the bars and equilibrated forces on each interface of the sample. The dynamic forces on the incident bar-sample interface P_1 and that on the transmitted bar-sample interface P_2 are

$$P_1 = EA(\varepsilon_i + \varepsilon_r), P_2 = EA\varepsilon_t \tag{1}$$

The stress (σ_s), strain rate ($\dot{\varepsilon}_s$), and strain histories (ε_s) in the sample are as follows:

$$\sigma_s(t) = E\frac{A}{A_s}\varepsilon_t(t) \tag{2}$$

$$\dot{\varepsilon}_s(t) = -2C\frac{\varepsilon_r(t)}{L_s} \tag{3}$$

$$\varepsilon_s(t) = \int_0^t \left(-2C\frac{\varepsilon_r(\tau)}{L_s}\right)d\tau \tag{4}$$

where E and C are the Young's modulus and wave speed of the bar material, respectively, A is the cross-sectional area of the incident or transmitted bar, L_s is the original length of the specimen and A_s is the cross-sectional area of the sample (which is equal to A in the current case). ε_t and ε_r are the strains measured from transmitted and reflected waves, respectively. In the current case, E is 200 GPa and C is 4790 m/s.

Copper and rubber pulse shapers were used between the striker and incident bars to ensure that the strain rate of the sample remains relatively constant during the loading portion of the test and to ensure the force equilibrium on each interface of the sample. This pulse shaper technique has been extensively used in SHPB tests [18, 19].

Specimen Preparation

For the dry sand testing, the sample is placed within the maraging steel tube and sandwiched between two steel platens having a diameter of 25.35 mm and a length of 15.0 mm, which secure the sand in the axial direction. There is a 0.05-mm gap between the diameter of the steel platens and the steel sleeve to eliminate the friction between the platens and sleeve and guarantee the accuracy of the dynamic sand compression tests. The gap also allows air to escape during the dynamic tests. For assembly, one steel platen is placed within the tube and is fixed by two screws (see Fig. 4a). Dry sand is poured into the tube, with total masses of 1, 2, 4, and 6 g for the dynamic tests and 8 g for the quasi-static test (see Fig. 4b). Thereafter, the opposite platen is pressed inside the tube from the opposite end without fixing. The total assembly and sand are shaken automatically using a shaking apparatus to consolidate the sand sample to obtain different initial bulk densities. The duration for which the sand and assembly are shaken is controlled. When the desirable length of the sand sample is reached, the platen is fixed by another set of two screws (see
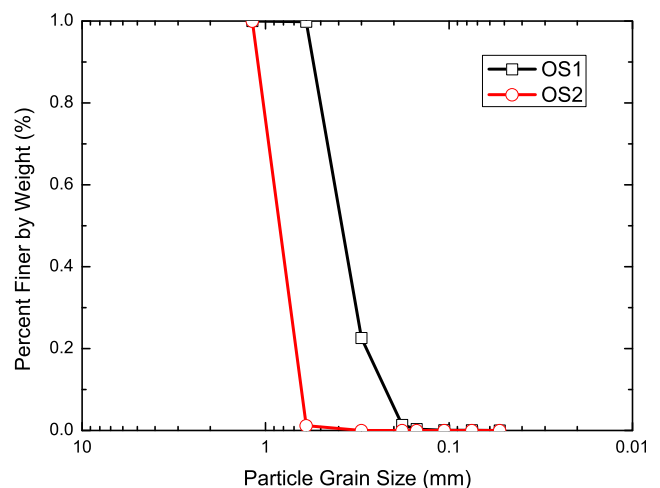

Fig. 2 Particle size distribution of the two types of Ottawa sand

Fig. 3 Schematic of the split
Hopkinson pressure bar for the
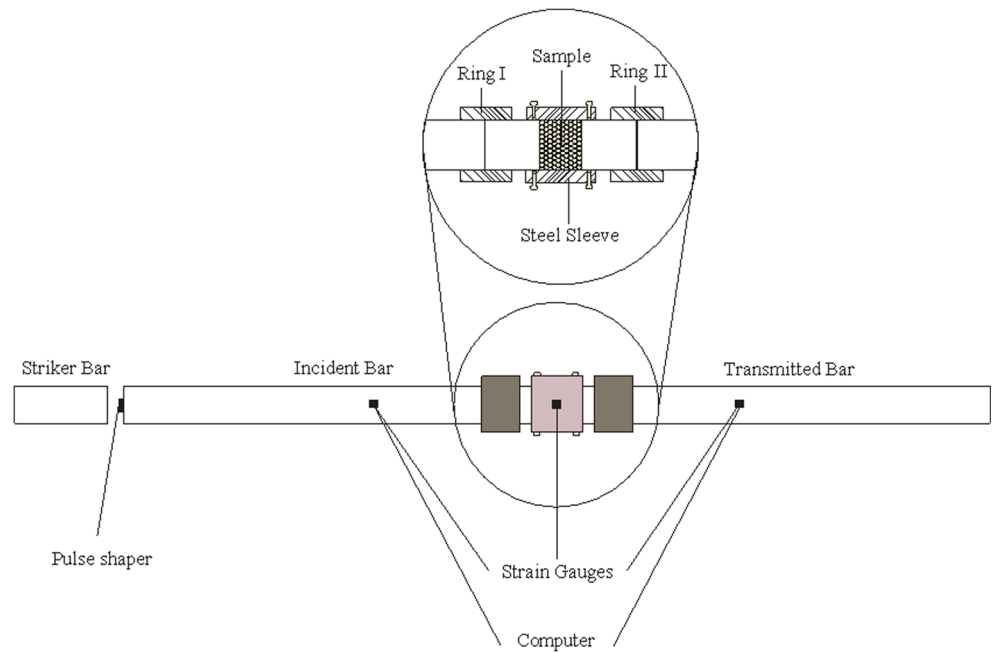dynamic compression test of sand

Fig. 4c), thus yielding the different initial bulk densities. This design is similar to that used by Song et al. [17].

According to the definition of the void ratio, $e = n/(1-n)$, where n is the porosity and equals $1-(V_s/V)$, V_s is the volume of the sand solid and V is the volume of the sand sample. Thus, the relation between the void ratio e and bulk density ρ_b of sands can be expressed as $e = (\rho/\rho_b) -1$, where ρ is the particle density of sand. The average sample dimensions and void ratios of the sand for dry tests are given in Table 2. The initial void ratio of the sand sample decreased with increasing sample mass due to the compaction process.

In addition to dry samples, sand samples with a high degree of saturation were also investigated. The assembly process of these samples is slightly different to accommodate excess water buildup within the sample. The first platen is solid, whereas the second platen contains two small grooves on its wall along the axial direction. First, the solid platen is placed in the tube

and fixed using two small screws (Fig. 4a). Second, water is added to a certain amount of sand until the water covers the surface of the sand. Finally, the new platen with two notches is placed inside the tube to discharge the excess water from the sample. A thin layer of vacuum grease is placed around each of the two complete platens to seal the water in the specimen during the preparation procedure. The OS1 samples contain an average of 1.06 g of water per 4 g of sand, and the OS2 samples contain an average of 1.05 g of water per 4 g of sand after removing the excess water. The saturation ratio of sands (R_s) is the volume of the contained water (V_w) divided by the volume of the voids (V_v), i.e., $R_s = V_w/V_v$. Thus, the degrees of saturation for the OS1 and OS2 samples are 0.97 and 0.99, respectively.

In the comparison static tests, the ring and platen sample assembly is directly placed on the testing platform, and in the SHPB test, the sample assembly is placed within the incident
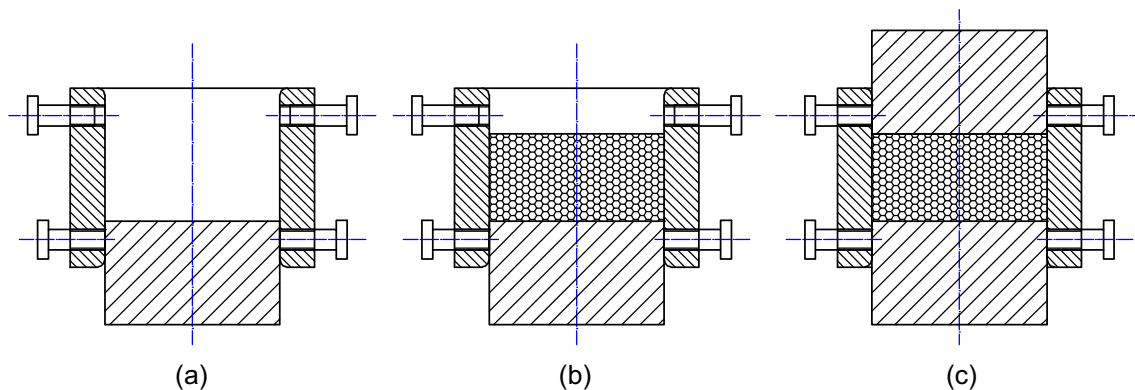

Fig. 4 Assembly procedure of the sand. (**a**) The first platen is fixed in the steel sleeve; (**b**) sand is placed in the sleeve; and (**c**) the second platen is inserted into the sleeve to confine the sand sample

Table 2 Dimensions of the dry sand specimens with different masses

Sand type	Mass (g)	Diameter (mm)	Average length (mm)	Average bulk density (g/cm^3)	Void ratio
OS1 (Dry)	1	25.4	1.37 (±0.05)	1.44 (±0.05)	0.83 (±0.02)
	2	25.4	2.62 (±0.09)	1.51 (±0.05)	0.75 (±0.02)
	4	25.4	5.04 (±0.13)	1.57 (±0.04)	0.68 (±0.02)
	6	25.4	7.44 (±0.27)	1.59 (±0.06)	0.66 (±0.02)
	8	25.4	9.75 (±0.31)	1.62 (±0.05)	0.63 (±0.02)
OS2 (Dry)	1	25.4	1.38 (±0.03)	1.43 (±0.03)	0.86 (±0.01)
	2	25.4	2.61 (±0.04)	1.51 (±0.03)	0.75 (±0.01)
	4	25.4	5.08 (±0.16)	1.55 (±0.05)	0.71 (±0.02)
	6	25.4	7.39 (±0.14)	1.60 (±0.03)	0.66 (±0.01)
	8	25.4	9.76 (±0.27)	1.62 (±0.05)	0.64 (±0.02)

and transmitted bars. The interface between the assembly platen and incident bar is glued to ensure the transmission of tensile waves through the system. A thin layer of vacuum grease is used at the platen-transmitted bar interface, where the load is always compressive, to ensure good contact. Before impact, the positioning screws are loosened to allow for the free movement of the loading platens.

Dynamic Force Balance and Constant Strain Rate

The pulse shaper technique was used to condition the loading wave created by the striker bar in the SHPB setup. The reasons for this approach are twofold: first, the forces at each sample interface must be simultaneously equal in magnitude to maintain a uniform deformation field within the sample; and second, a constant strain rate is desired to investigate the overall load-deformation response at that particular strain rate, and a constant strain rate can be achieved with proper pulse shaping [20].

Typical oscilloscope records are presented in Fig. 5. The reflected wave is flat (after a ramp-up period), which indicates that a constant strain rate has been achieved (see Equation 3). Figure 6 shows the forces at both ends of the specimen for the same two tests in Fig. 5 using Eq. 1. These two graphs illustrate that the condition of dynamic force balance has been achieved. In addition, as shown in Fig. 3, a strain gauge is circumferentially mounted on the surface of the confinement steel sleeve. The radial strain of the steel sleeve during the dynamic loading is measured. The radial signals measured from the confinement maraging steel sleeve are often influenced by irregular electromagnetic interference [21]. Hence, according the method proposed by Barr et al. [21], the strain gauge lead wires were twisted and aligned with the magnetic field lines around the bar and sleeve to minimize the electromagnetic interference in the strain gauge signals. Typical signals of this strain gauge are shown in Fig. 5c, which illustrates that the radial strain of the sleeve is small and can be neglected.

Many tests were conducted on individual samples with the same testing parameters due to the variability that is inherent in the sand sample and the variations in the experimental procedure. Each test was repeated at least ten times for samples of the same size and type at a given strain rate. Of these 10 datasets, those within similar results were chosen, and their average was considered the stress-strain behavior of the sample. Figure 7 shows the results of the repeated tests for OS1 and OS2 under strain rates of 820 s^{-1} and 830 s^{-1}, respectively. The averaged stress-strain curves and their standard deviations are also shown in Fig. 7.

Results and Discussion

Quasi-static Behavior of Dry Sands

A series of quasi-static tests were conducted with an MTS hydraulic servo-controlled testing system. In the tests, the loading rate was set at 0.008 mm/s, and the sample weight was approximately 8 g. The mean curve taken from the tests is shown in Fig. 8. The transition of deformation caused by particle crushing is more pronounced for OS2, which is expected because this sand has a larger average particle size. Once crushing of the particles has begun, the moduli of OS1 and OS2 increase appreciably as the void spaces are depleted and approach the stiffness of a fully confined quartz material.

Rate Dependence of Dry Sands

Following the procedure outlined in Section 2, SHPB tests for dry OS1 sand were conducted on samples with masses of 1, 2, 4, and 6 g. The different initial void ratios were achieved using the different sample thicknesses (given in Table 2). For each mass, several stress-strain curves were obtained at various strain rates by averaging over several
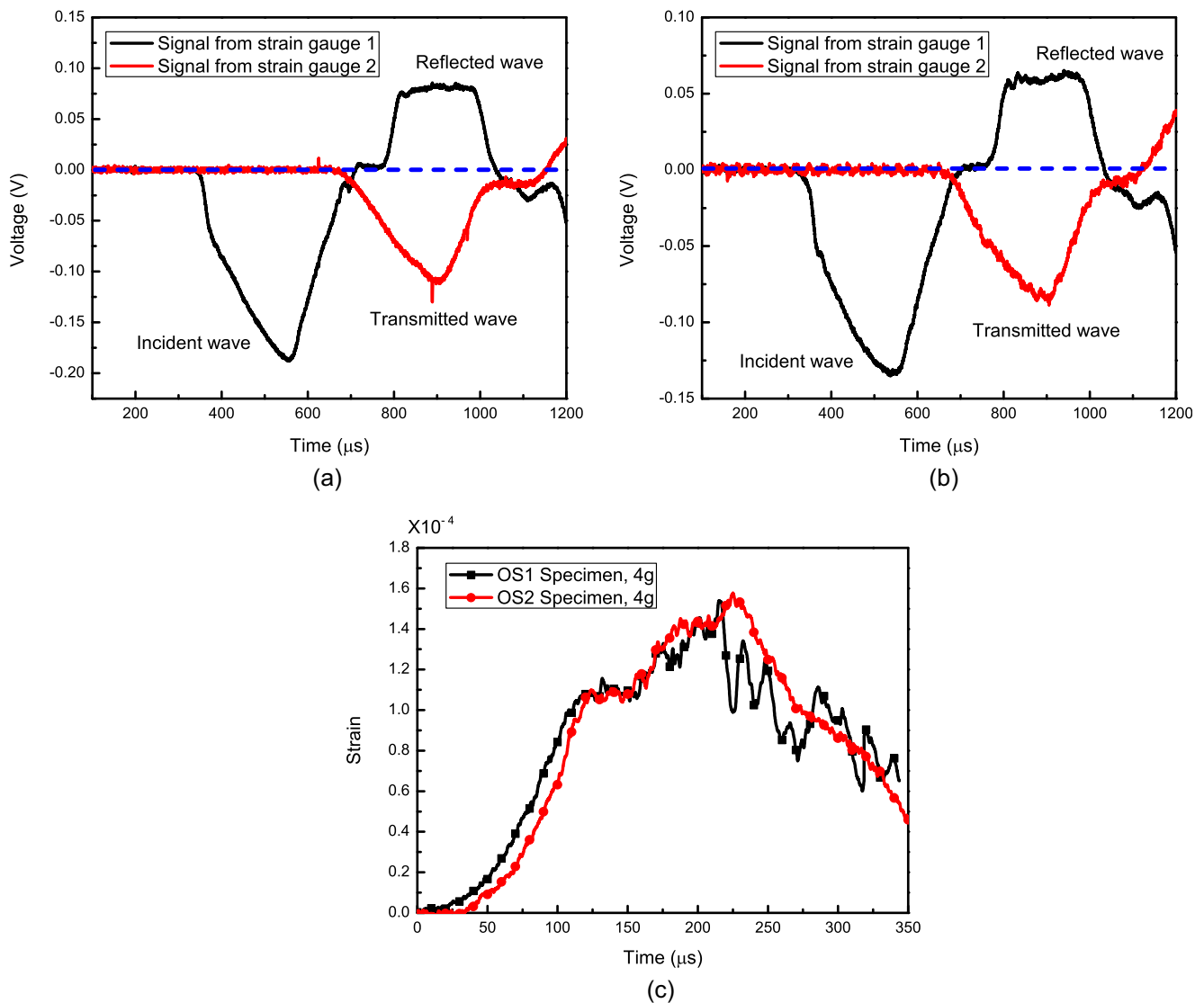
Fig. 5 (**a**)Typical oscilloscope record (high strain rate, 4 g dry OS1 specimen, void ratio of 0.68); (**b**) Typical oscilloscope record (low strain rate, 4 g dry OS2 specimen, void ratio of 0.71). (**c**) Typical radial strains of the steel sleeve

tests. The stress-strain curves for each initial void ratio are shown in Fig. 9, which illustrates that the stress-strain response is not strongly influenced by the strain rate, particularly at lower strains. A certain degree of rate dependence is observed toward higher strains, for example, above 0.15 in Figs. 9a–c. Felice et al. [22] concluded that the initial gas porosity of the soil is a principal parameter governing the stress-strain response. In addition, they found that the resultant stress-strain response is insensitive to the strain rate when the strain is less than the initial gas porosity. Furthermore, a noisier signal is obtained for the 6 g samples (Fig. 9d), indicating that tests on larger samples are less repeatable and consistent. The response is linear at lower strains, whereas the sample stiffens at higher strains, likely resulting from compaction as the void spaces are depleted. These results are consistent with those reported by Song

et al. [17]. Moreover, the stress-strain curves for all void ratios have a similar tendency at strains less than 0.15, i.e., the stress increases nearly linearly with the strain. For the samples with higher void ratios (0.83, 0.75 and 0.68), the rate dependency and stiffened part in the stress-strain curves are all observed when the strain is above 0.15. For the samples with a void ratio of 0.66, the highest strain in Fig. 9d is approximately 0.15, and thus, the stiffened part in the stress-strain curve does not appear. Therefore, under highly similar strain rates, the tendency of the stress-strain curve at strains of less than 0.15 is not influenced by the void ratios, and the stress-strain curve at strains above 0.15 exhibits a similar rate dependency and stiffened part for all void ratios.

The results for the coarse-grained OS2 sand in the dry condition are presented in Fig. 10. Similar to the results
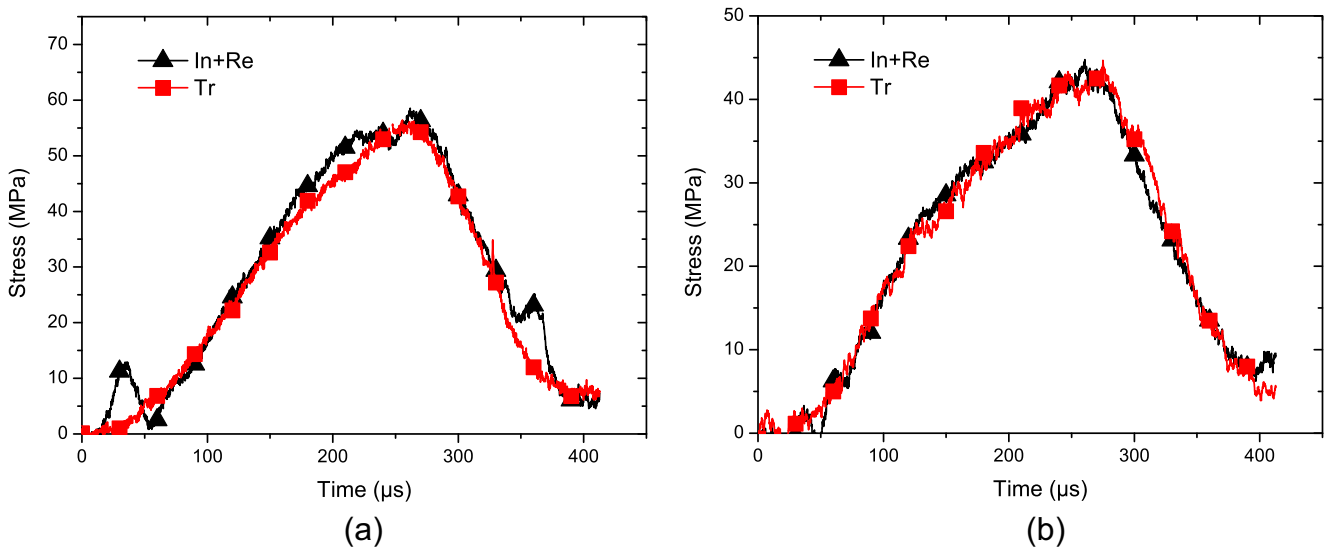
Fig. 6 Stress balance histories from two typical tests. (**a**) 4 g dry OS1 specimen, void ratio of 0.68; (**b**) 4 g dry OS2 specimen, void ratio of 0.71

from the dry OS1 tests, the samples exhibit limited strain rate dependency, particularly at lower strains. However, a certain degree of strain rate dependency is observed at larger strains (above 0.16). Namely, the stress-strain curves for all void ratios have a similar tendency at strains of less than 0.16. For samples with higher void ratios (0.86, 0.75 and 0.71), the rate dependency and stiffened part in the stress-strain curves are all observed when the strain is higher than 0.16. For the samples with a void ratio of 0.66, the highest strain in Fig. 10d is less than 0.16, and thus, the stiffened part in the stress-strain curve is not apparent. Therefore, under highly similar strain rates, the tendency of the stress-strain curve at strains less than 0.16 is not influenced by the void ratios, and the stress-strain curve at strains higher than 0.16 exhibits a similar rate dependency

and stiffened part for all void ratios. The slight difference in the critical strains of OS1 and OS2 for the strain rate dependency observed may be caused by the different void ratios and particle size distributions of the two types of sand.

As discussed in the introduction, the static stress-strain curve in uniaxial strain tests of sand can be characterized by four stages according to Omidvar et al. [2]: the initial elastic stage; particle rearrangement at low confining pressure; particle crushing and rearranging under higher stress; and at extremely high stress, the crushed particles are in increased contact, resulting in a pseudo-elastic behavior approaching that of quartzite. It is not clear why the sand considered here does not exhibit significant rate dependency at lower strains, whereas rate dependency can be observed at higher strains. Despite
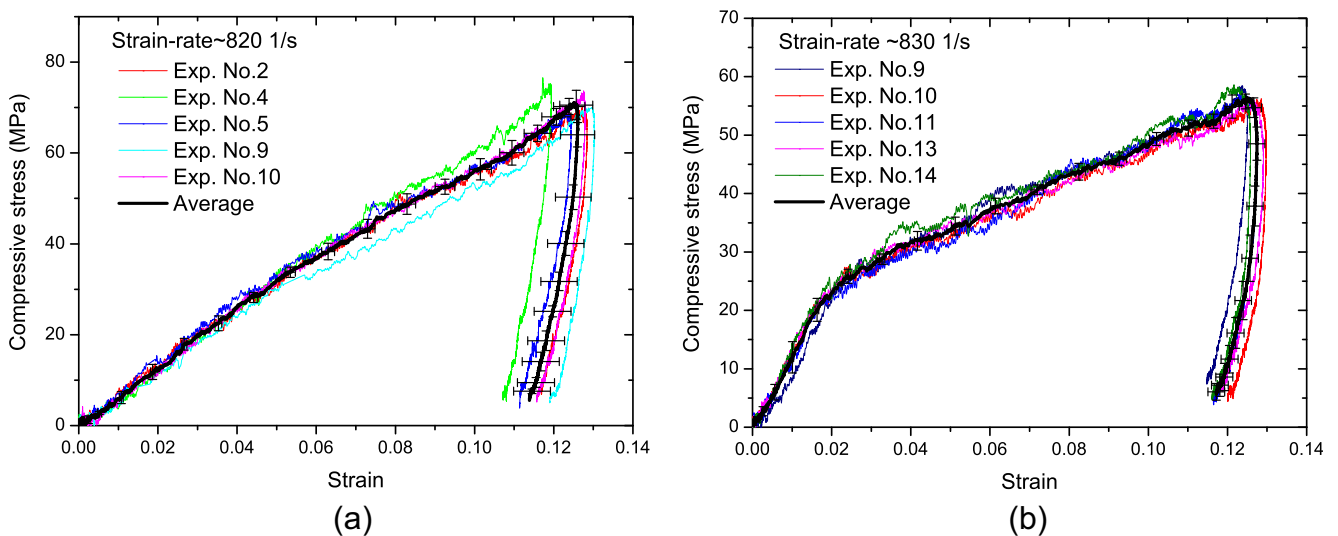

Fig. 7 Multiple and average dynamic stress-strain curves for (**a**) dry, void ratio of 0.68, 4 g OS1 sample; and (**b**) dry, void ratio of 0.71, 4 g OS2 sample
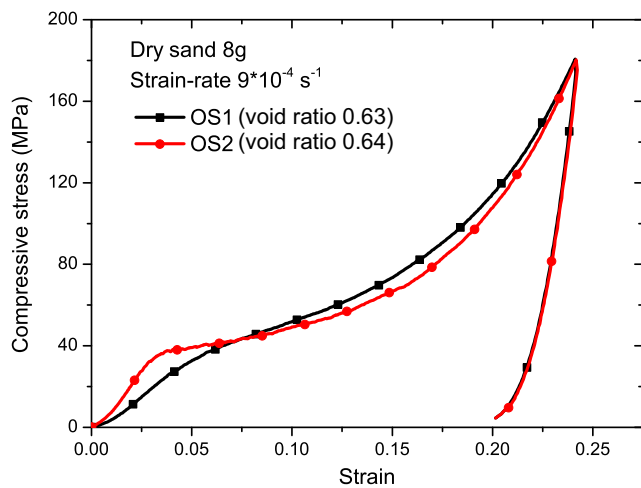
Fig. 8 Static stress-strain curves of dry sand specimens

different researchers' attempts [9, 23], this issue has not been addressed in full, and more research and experimental tests are needed. In addition, similar to the OS1 samples, the OS2

samples exhibit linear behavior toward lower strains and stiffening toward higher strains. The 6 g samples are noisier and less consistent than the smaller samples.

Solid-like and fluid-like Behaviors of Dry Sand

According to the stress-strain curves for dry OS1 and OS2 sand, two types of dynamic behaviors are observed in the dry sand: solid-like and fluid-like behavior (see Fig. 11). In the solid-like response (Fig. 11a), there are three zones in the entire stress-strain curve. In Zone 1, the sand response becomes stiffer due to the enhanced friction between sand particles. This phase is known as an initial elastic response. Zone 2 is the yielding of the sand skeleton, in which the stress increases linearly with the strain. A hardening and lock-up phase dominates Zone 3, which is characterized by an increase in stiffness relative to the yielding phase. The stress-strain curves of dry OS2 sand with all initial void ratios belongs to solid-like behavior. As shown in Fig. 10, there are three corresponding
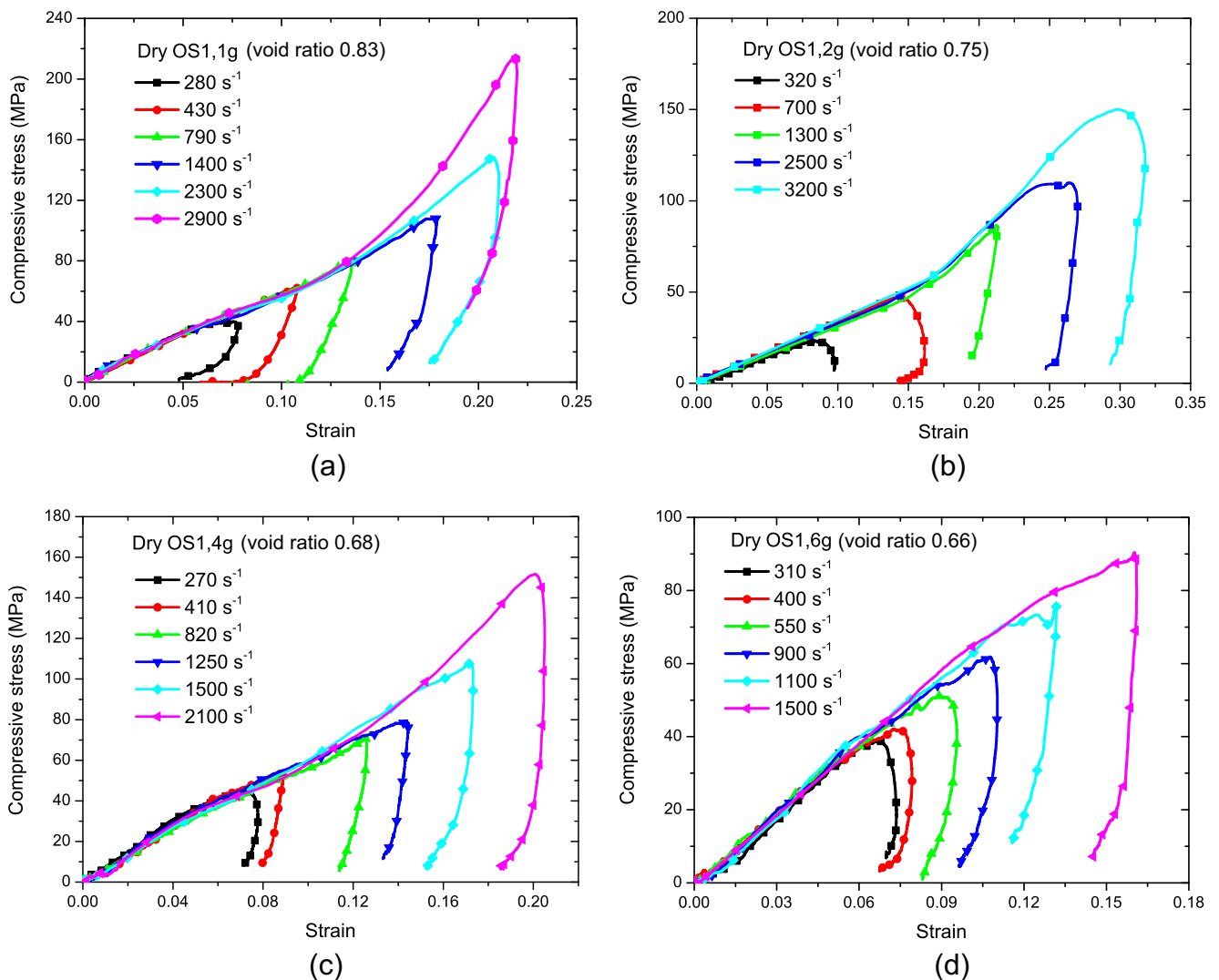

Fig. 9 Dynamic stress-strain curves of the dry OS1 specimens. (**a**) Void ratio of 0.83; (**b**) void ratio of 0.75; (**c**) void ratio of 0.68 and (**d**) void ratio of 0.66
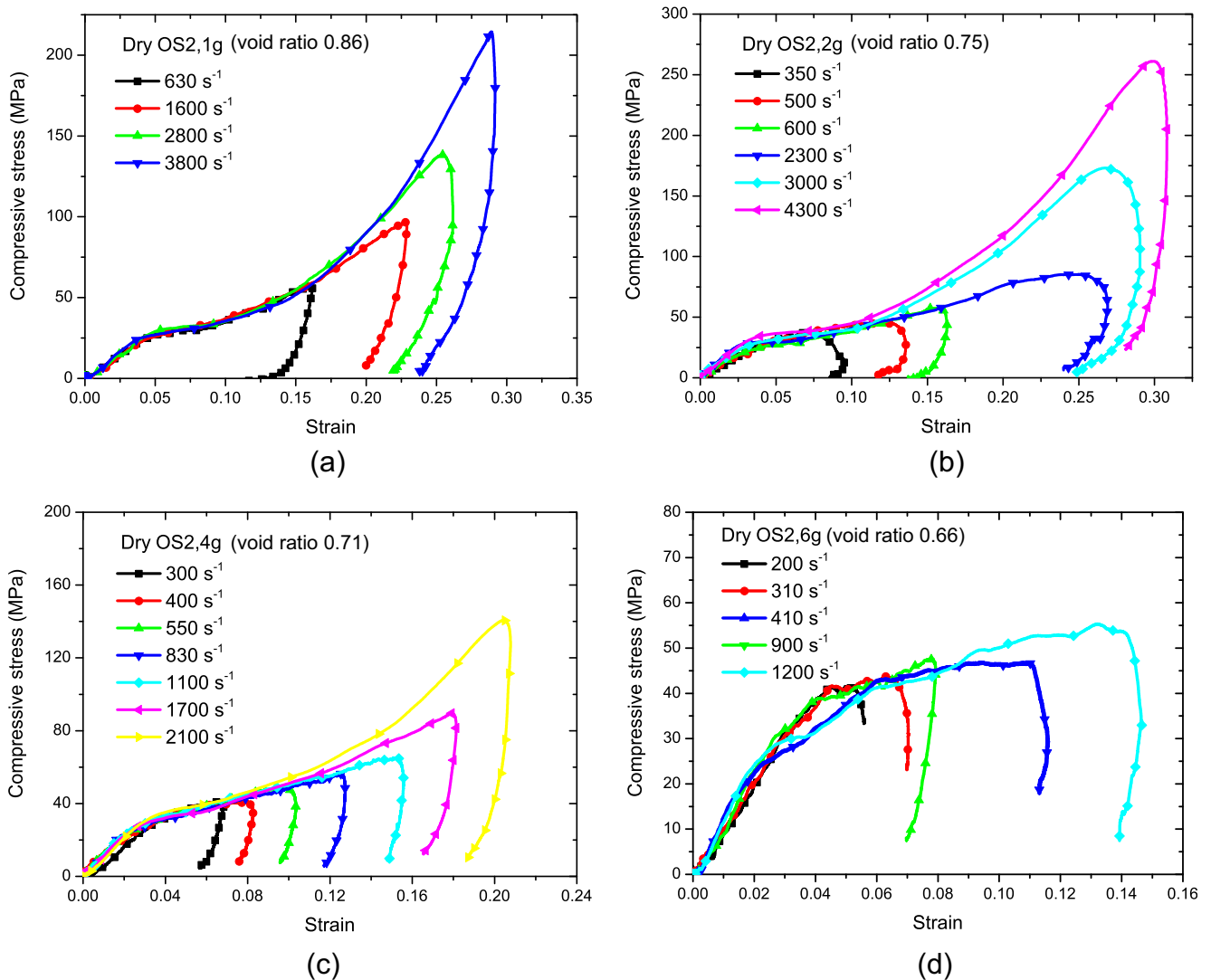
Fig. 10 Dynamic stress-strain curves of the dry OS2 specimens. (**a**) Void ratio of 0.86; (**b**) void ratio of 0.75; (**c**) void ratio of 0.71 and (**d**) void ratio of 0.66

zones: the initial elastic stage (Zone 1); particle rearrangement (Zone 2); and particle crushing and rearranging (Zone 3).

In the fluid-like behavior (Fig. 11b), Zone 1 is gone, and the entire stress-strain curves are composed of Zones 2 and 3. This fluid-like response is unique to the dynamic response of granular materials and is likely due to a fluidization (i.e., loss of shear resistance) resulting from certain harmonic frequencies at the length scale of the sample in question, as proposed by Melosh [24] and Melosh [25]. He proposed that dynamic stressing at the acoustic frequencies of a granular material could generate internal stresses that can reduce the effective normal stress caused by material weakening. Relatively little laboratory work has been conducted to study this phenomenon. Xia et al. [26] observed and described this phenomenon in a laboratory-scale test on finely crushed rock particles from mine tailings (for a detailed description, see Xia et al. [26]).

For OS1, the fluidization response of sand occurs at all initial void ratios of sand samples in dynamic loading. The static response of OS1 is solid-like, and all dynamic responses of OS1 are fluid-like. However, the OS2 samples for all void ratios in this study exhibit a solid-like response regardless of the nature of the load; thus, fluidization does not occur for this sand. This difference in the responses of the two sands may result from the difference in the particle size distributions of OS1 and OS2. The particle size distribution of OS1 is larger than that of OS2. A wider particle size distribution results in a higher possibility of fluidization of the sand [26]. In addition, for sand with a larger particle size, the smaller fragments fractured from large particles are likely to fill in the gaps between larger sand grains to provide resistance for compression [27]. Thus, fluidization occurs in OS1 but not in OS2. In addition, the stress-strain curves of sand obtained by Song et al. [17] are also similar to those shown in Fig. 11b because the sand

Fig. 11 (**a**) Solid-like and (**b**) fluid-like behaviors of dry sand under uniaxial strain loading


(a)

(b)
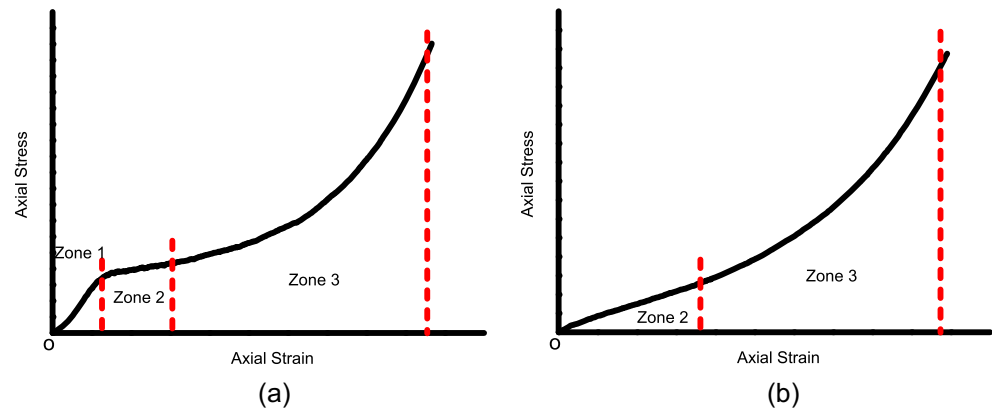
considered by Song et al. [17] has a wide particle size distribution. As a result, the particle size distribution influences the fluidization (a breakdown of shear stresses) response of sand. The optical morphology images of OS1 and OS2 before and after the typical dynamic compression test are shown in Fig. 12. This figure illustrates that a considerably large number of sand grains have been fractured. The irregular fragments with sharp edges have been formed, and some sand grains have been pulverized. Compared with the fractured grains in OS1, more irregular fractured and pulverized grains are found in OS2. Thus, those images support the above discussion of the stress-strain behavior of the two sands.

Rate Dependence of Saturated Sands

The results of the saturated sand samples are shown in Fig. 13. Here, 4 g OS1 and OS2 samples were tested under a high degree of saturation. The results indicate that the presence of water significantly increases the stiffness of the sample. This phenomenon is consistent with the results reported by Luo et al. [27], who studied the effect of saturation level (water contents of 0–16.5%) on the triaxial stress-strain behavior of sand and indicated that partially saturated sand appears stiffer than dry sand. Luo et al. [27] also demonstrated that the stress-strain curves for different saturation

Fig. 12 Optical morphology images of (**a**) OS1 sand before the test; (**b**) OS2 sand before the test; (**c**) OS1 sand after the test (void ratio of 0.66, strain rate of 900 s^{-1}); (**d**) OS2 sand after the test (void ratio of 0.66, strain rate of 900 s^{-1})
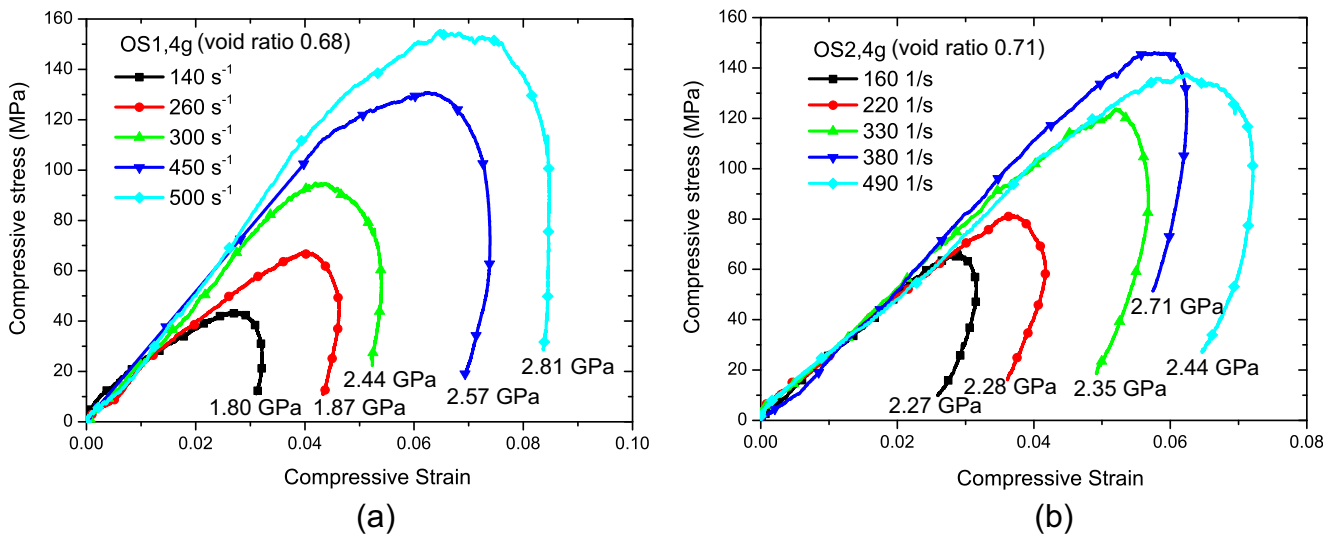

(a)

(b)

(c)

(d)
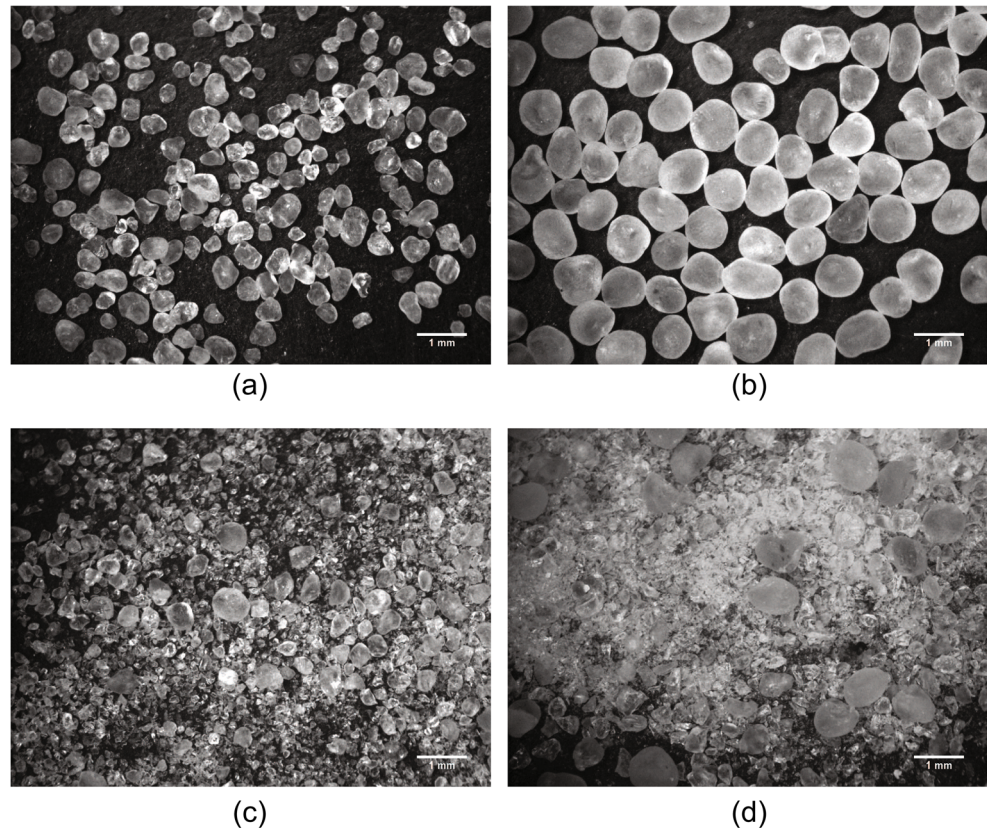
Fig. 13 Stress-strain curves of the fully saturated sand specimens. (**a**) OS1; (**b**) OS2

levels are highly similar to each other at compressive strains of 2–4% and that the difference becomes significant at strains larger than 5%. Furthermore, in Fig. 13, the stress-strain response is remarkably linear and rate dependent, with the stiffness increasing with increasing strain rates. (The moduli of elasticity are shown in Fig. 13.) The strong strain rate dependency can be attributed to the limited amount of time that the particles have been available to rearrange, thus resulting in a higher stiffness for higher strain rates.

The deformation response of the saturated OS1 and OS2 samples is governed by the presence of water (which has a considerably lower compressibility than the soil skeleton) occupying the entirety of the void space (see Fig. 14). The water, which is effectively undrained due to the rapidly increasing loading pulse, accommodates the majority of the hydrostatic stress within the sample, resulting in a near-linear response. The strain rate has a pronounced

Fig. 14 Comparison between the stress-strain curves of saturated OS1 and OS2 sand

effect on the stiffness of the sample, which is likely explained by the rate at which sand particles deform and undergo rearrangement.

Conclusion

In this series of experiments, two types of Ottawa sand (ASTM C778 #20–30 graded sand (OS1) and C109 ASTM #C778 graded sand (OS2)) were tested in a systematic series of uniaxial strain experiments. The effects of the strain rate, initial void ratio and degree of saturation were examined.

Two types of dynamic behaviors were observed in the dry sand for all initial void ratios: solid-like and fluid-like behavior. Fluidization occurred at all initial void ratios for the OS1 sand samples. However, the OS2 samples exhibited only a solid-like response for all void ratios. This difference may result from the different particular size distributions of OS1 and OS2.

For the dry OS1 and OS2 samples, the initial elastic response and initial yielding of the sand skeleton zone seemed to be independent of the strain rate for all initial void ratios. The strain rate effects became more apparent after particle crushing and particle rearrangement began. In future studies, the SHPB method should be modified to provide both longer and faster loading pulses to reach a higher absolute strain (above 20%) and higher strain rates within the sample. These improvements would provide further insights into the material behavior under more extreme conditions.

Under a high degree of saturation, the strain rate effects were immediately apparent, even at lower strains. The undrained, dynamic response of sand was remarkably linear until the peak strain was attained.
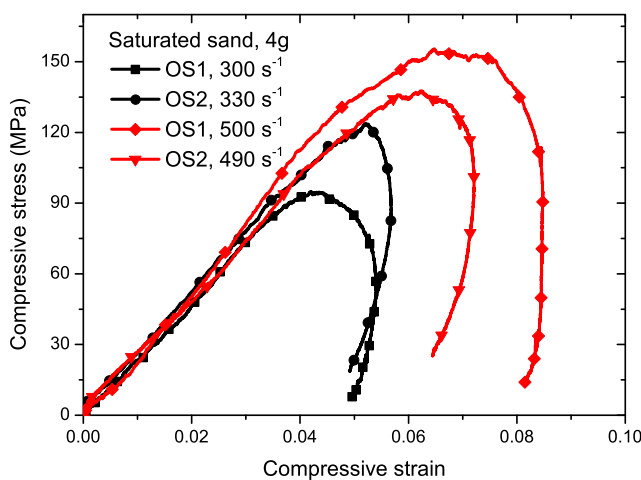
References

1. Meyers MA (1994) Dynamic behavior of materials. John wiley & sons, Trenton

2. Omidvar M, Iskander M, Bless S (2012) Stress-strain behavior of sand at high strain rates. Int J Impact Eng 49:192–213. doi:10.1016/j.ijimpeng.2012.03.004

3. Heierli W (1962) Inelastic wave propagation in soil columns. J Soil Mech Found Div Am Soc Civ Eng 88(SM6):33–63

4. Sparrow RW, Tory AC (1966) Behavior of a soil mass under dynamic loading. J Soil Mech Found Div ASCE 92(SM3):59–83

5. Whitman RV (1970) The Response of Soils to Dynamic Loadings; Report 26, Final Report. DTIC Document, Massachusetts Inst of Tech Cambridge Dept Of Civil Engineering

6. Jackson Jr JG, Ehrgott JQ, Rohani B (1979) Loading rate effects on compressibility of sand. DTIC Document, Army Engineer Waterways Experiment Station Vicksburg Ms Structures Lab

7. Lu H, Luo H, Komaduri R (2009) Dynamic compressive response of sand under confinements. In: 2009 SEM 2009 Annual Conference & Exposition on Experimental & Applied Mechanics. Albuquerque New Mexico USA, p 53

8. Luo H, Lu H, Cooper W, Komanduri R (2011) Effect of mass density on the compressive behavior of dry sand under confinement at high strain rates. Exp Mech 51(9):1499–1510

9. Parab ND, Claus B, Hudspeth MC, Black JT, Mondal A, Sun J, Fezzaa K, Xiao X, Luo SN, Chen W (2014) Experimental assessment of fracture of individual sand particles at different loading rates. Int J Impact Eng 68:8–14. doi:10.1016/j.ijimpeng.2014.01.003

10. Bragov AM, Lomunov AK, Sergeichev IV, Tsembelis K, Proud WG (2008) Determination of physicomechanical properties of soft soils from medium to high strain rates. Int J Impact Eng 35(9):967–976. doi:10.1016/j.ijimpeng.2007.07.004

11. Bragov AM, Kotov VL, Lomunov AK, Sergeichev IV (2004) Measurement of the Dynamic Characteristics of Soft Soils Using the Kolsky Method. J Appl Mech Tech Phys 45(4):580–585. doi:10.1023/B:JAMT.0000030338.66701.e9

12. Bragov AM, Lomunov AK, Sergeichev IV, Proud W, Tsembelis K, Church P (2005) A method for determining the main mechanical properties of soft soils at high strain rates (10^3–10^5 s^{-1}) and load

13. Bragov AM, Grushevsky GM, Lomunov AK (1996) Use of the Kolsky method for confined tests of soft soils. Exp Mech 36(3):237–242. doi:10.1007/BF02318013

14. Pierce S, Charlie W (1989) High-intensity compressive stress wave propagation through unsaturated sands. DTIC Document, Colorado State Univ Fort Collins

15. Martin BE, Chen W, Song B, Akers SA (2009) Moisture effects on the high strain-rate behavior of sand. Mech Mater 41(6):786–798. doi:10.1016/j.mechmat.2009.01.014

16. Kabir E, Chen W (2011) Sand Particle Breakage under High-Pressure and High-Rate Loading. In: Proulx T (ed) Dynamic Behavior of Materials, Volume 1. Conference Proceedings of the Society for Experimental Mechanics Series. Springer New York, pp 93–94. doi:10.1007/978-1-4614-0216-9_12

17. Song B, Chen W, Luk V (2009) Impact compressive response of dry sand. Mech Mater 41(6):777–785

18. Frew D, Forrestal M, Chen W (2002) Pulse shaping techniques for testing brittle materials with a split Hopkinson pressure bar. Exp Mech 42(1):93–106. doi:10.1007/bf02411056

19. Xia K, Nasseri MHB, Mohanty B, Lu F, Chen R, Luo SN (2008) Effects of microstructures on dynamic compression of barre granite. Int J Rock Mech Min Sci 45(6):879–887. doi:10.1016/j.ijrmms.2007.09.013

20. Frew DJ, Forrestal MJ, Chen W (2001) A split Hopkinson pressure bar technique to determine compressive stress-strain data for rock materials. Exp Mech 41(1):40–46. doi:10.1007/bf02323102

21. Barr AD, Clarke SD, Tyas A, Warren JA (2017) Electromagnetic Interference in Measurements of Radial Stress During Split Hopkinson Pressure Bar Experiments. Exp Mech 57(5):813–817. doi:10.1007/s11340-017-0280-4

22. Felice CW, Gaffney ES, Brown JA, Olsen JM (1987) Dynamic high stress experiments on soil. Geotech Test J 10(4):192–202

23. Huang J, Xu S, Hu S (2014) Influence of particle breakage on the dynamic compression responses of brittle granular materials. Mech Mater 68:15–28. doi:10.1016/j.mechmat.2013.08.002

24. Melosh HJ (1979) Acoustic fluidization: A new geologic process? J Geophys Res Solid Earth 84(B13):7513–7520. doi:10.1029/JB084iB13p07513

25. Melosh HJ (1996) Dynamical weakening of faults by acoustic fluidization. Nature 379(6566):601–606

26. Xia K, Huang S, Marone C (2013) Laboratory observation of acoustic fluidization in granular fault gouge and implications for dynamic weakening of earthquake faults. Geochem Geophys Geosyst 14(4):1012–1022. doi:10.1002/ggge.20076

27. Luo H, Cooper WL, Lu H (2014) Effects of particle size and moisture on the compressive behavior of dense Eglin sand under confinement at high strain rates. Int J Impact Eng 65:40–55. doi:10.1016/j.ijimpeng.2013.11.001